Journal of Dental Sciences (2016) 11, 156–163

Available online at www.sciencedirect.com

ScienceDirect

journal homepage: www.e-jds.com

ORIGINAL ARTICLE

Interfacial analysis of porcelain fused to high-palladium alloy with different observation methods

Hao-Sheng Chang [a,b], Chao-Sen Yang [c], Yao-Dung Hsieh [d], Ming Chen [c*]

[a] Department of Stomatology, Kaohsiung Veteran General Hospital, Kaohsiung, Taiwan
[b] Department of Dental Technology, Shu-Zen Junior College of Medicine and Management, Kaohsiung, Taiwan
[c] Department of Materials and Optoelectronic Science, National Sun Yat-sen University, Kaohsiung, Taiwan
[d] Kaohsiung Veteran General Hospital, Pingtung Branch, Pingtung, Taiwan

Received 15 June 2015; Final revision received 3 October 2015
Available online 5 January 2016

KEYWORDS
electron probe microanalysis;
palladium–silver alloy;
scanning electron microscopy combined with energy dispersive X-ray analysis;
X-ray photoelectron spectroscopy

Abstract *Background/purpose:* In a previous fractural study of implant-supported crowns, it was found that the palladium–silver crowns possessed the highest fracture force. The ceramic–metal interface was examined to explain its high resistance to fracture.
Materials and methods: Palladium–silver crowns with the morphology of a maxillary second premolar were prepared following standard dental laboratory procedures. Crown specimens were compressed vertically in the center of the occlusal surface until fracture, using a universal testing machine. The fractured surfaces were examined using scanning electron microscopy combined with energy dispersive X-ray spectroscopy to determine the failure mode. The ceramic–metal interface of the crown was examined with electron probe microanalysis. Additionally, sheet specimens with a dimension of $10 \times 9 \times 4$ mm^3 were prepared to examine the surface morphology and composition of palladium–silver alloy after oxidation and porcelain-fused-to-metal firing cycles.
Results: The average fracture force was 1425 ± 392N. Analyses with scanning electron microscopy combined with energy dispersive X-ray spectroscopy revealed that the failure mode was cohesive within the ceramic layer. Electron probe microanalysis micrographs indicated that Sn and In were found to distribute only on the alloy side of the ceramometal crown. Energy dispersive X-ray spectroscopy analysis and electron probe microanalysis micrographs confirmed that ZnO had diffused into the ceramic phase.
Conclusion: In_2O_3, SnO_2, and ZnO were found along the interface; the presence of these oxides at the boundary promotes ceramic–metal adhesion, and this resulted in cohesive failure of the

* Corresponding author. Department of Materials and Optoelectronic Science, National Sun Yat-sen University, 70 Lien-Hai Road, Kaohsiung 80424, Taiwan.
E-mail address: mingchen@faculty.nsysu.edu.tw (M. Chen).

http://dx.doi.org/10.1016/j.jds.2015.10.001

ceramic layer. ZnO was found to diffuse into the ceramic phase, and it is suggested to be beneficial for high fracture resistance in the present study.

Introduction

Palladium—silver (Pd—Ag) alloys were first introduced for dental restorations in the 1970s as an alternative to costly gold-based dental alloys.[1,2] Commercially relevant Pd—Ag alloys typically have compositions of approximately 50—60% Pd and 30—40% Ag, and contain small amounts of low-melting-point metals, such as Zn, In, and Sn, to improve castability by increasing the fluidity of the molten alloy.[3] Adherence of porcelain to noble alloys is usually improved by adding easily oxidized alloy components, such as In, Sn, and Ga.[4—6] Accumulation of these elements at the metal—ceramic interface has been reported in several studies.[7—10] The bonding mechanism is believed to result from suitable oxidation of the metal[11—14] and diffusion of the oxides into the opaque porcelain during firing.

Porcelain fracture related to an implant-supported porcelain-fused-to-metal (PFM) crown or bridge was found to have a significantly higher risk than that of tooth-supported restorations.[15] It was previously thought that biological or mechanical factors were the dominant causes of failure after PFM crown restoration.[16] Studies using three or four points, and double bending tests to measure bonding strength between porcelain and metal coping were unable to accurately imitate the failure mode of a PFM crown under actual oral conditions.[17,18] Many PFM crown restoration casts were developed, and the Instron testing machine was introduced to determine PFM crown fracture resistance.[19,20] In a recent fractural study of implant-supported crowns that were porcelain-fused to five different commercial alloys,[21] it was determined that the Pd—Ag alloy had the highest fracture force. Still more detailed information is required on such a high Pd—Ag alloy commercial product in PFM crown restoration. The aim of this study is to find out the interface characteristics after PFM firing cycles, using multitechnique analysis methods, including X-ray photoelectron spectroscopy (XPS), scanning electron microscopy combined with energy dispersive X-ray analysis (SEM/EDX), and electron probe microanalysis (EPMA), for characterizing the alloy surface after oxidation and the ceramic—metal interface after PFM firing cycles. Failure modes of fractured surfaces were determined using SEM/EDX and EPMA.

Materials and methods

Specimen preparation

The materials used in this study were Pd—Ag dental casting alloys (Argelite 50; Argen Corporation, San Diego, CA, USA) with compositions shown in column 2 of Table 1. Au and Ru were present as trace elements (each $<$ 1 wt%). Uniform ceramometal crowns of a Pd—Ag alloy, with equivalent morphologies to the maxillary second premolar, were duplicated on a Straumann straight screw-retained abutment (Lot No.: 048.605; Straumann, Basel, Switzerland) connected to a Straumann regular neck tissue-leveled implant analog (Lot No.: 048.124) under a 35N preload. Additionally, Pd—Ag alloy sheets with a dimension of $10 \times 9 \times 4$ mm^3 were prepared. Ten ceramometal crowns and six sheets of Pd—Ag alloy were fabricated following the manufacturer's instructions, involving five standard dental preparation stages (Figure 1):

(1) To make the castings, wax patterns were prepared, sprued, and invested with gypsum-bonded cristobalite investment material (Shofu Inc., Kyoto, Japan). The alloy was melted using a multiorifice gas-oxygen torch, cast into the mold using a centrifugal dental casting machine, and then bench cooled.
(2) After devesting, the alloy was blasted with 50 μm Al_2O_3 particles (Bego, Bremen, Germany).
(3) Specimens were grounded smoothly and were blasted again with 50 μm Al_2O_3 particles, and then the blasted surface was cleaned with steam.
(4) After surface treatment, the specimens were oxidized by heating them in a mild vacuum (10 mmHg) in a dental ceramic furnace (Programat P300; Ivoclar Vivadent Inc., Amherst, NY, USA) from 450°C to 1000°C at a rate of 45°C/min with a 1-minute hold at the peak temperature. The specimens were bench cooled to room temperature (RT). Three of these sheet specimens were left in this oxidized state. Their surfaces were first examined with XPS. SEM/EDX

Table 1 Bulk composition of Pd—Ag alloy as supplied by the manufacturer, surface composition obtained from EDX and XPS analyses after surface oxidation of the alloy, and surface composition of fractured crown on alloy side (in wt %).

	M[a]	EDX	XPS[b]	XPS	Upper[c]	Middle[c]	Lower[c]
Pd	49.6	21.6	0.9	1.0	47.3	46.0	39.5
Ag	40.0	28.0	1.2	1.3	41.1	45.4	41.7
In	5.0	27.7	49.8	57.0	0.0	0.0	0.0
Sn	4.0	12.6	17.4	20.6	0.0	0.0	0.0
Zn	1.0	10.1	30.8	20.1	11.7	8.6	18.8

EDX = energy dispersive X-ray analysis; XPS = X-ray photoelectron spectroscopy.
[a] Manufacture.
[b] Atom%.
[c] Obtained from EDX analysis on three different areas along the fracture path. Compositional data are expressed in wt% by adopting sum of Pd, Ag, In, Sn, and Zn as 100 wt%.

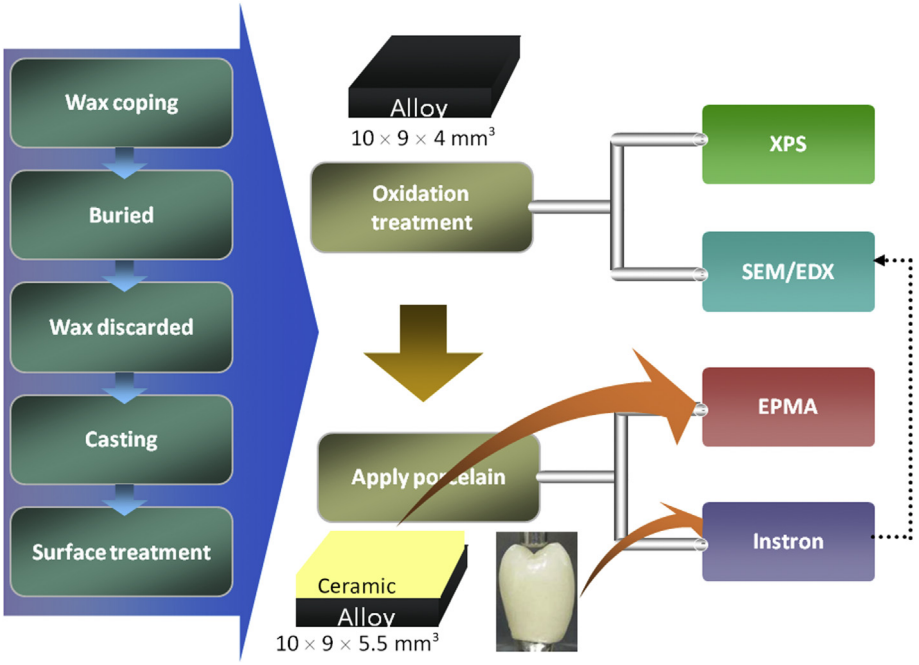

Figure 1 Schematic illustration of procedures for fabrication of rectangular specimens and crowns. Corresponding characterization is shown on right side. EDX = energy dispersive X-ray spectroscopy; EPMA = electron probe microanalysis; SEM = scanning electron microscopy; XPS = X-ray photoelectron spectroscopy.

was then used to analyze the surface morphology and composition of these three specimens.

(5) Fabrication of the crowns used eight-PFM firing cycles under a low vacuum of 10 mmHg in a dental ceramic furnace (Programat P300). Two layers of opaque dental porcelain (VITA VMK 68; Sirona Germany, Bensheim, Germany), with a combined thickness of 0.4 mm, were fired onto the crown surfaces by increasing the temperature from 600°C to 930°C over 3 minutes and holding at the peak temperature for 3 minutes for each firing cycle. Three layers of dentin porcelain (VITA VMK 95), with a combined thickness of approximately 1.0 mm, were fired onto the crowns by increasing the temperature from 600°C to 930°C over 6 minutes and holding at the peak temperature for 6 minutes. The crowns were bench set at RT after each firing cycle. The total porcelain thickness was approximately 1.4 mm. Two layers of glaze were fired onto the crowns by increasing the temperature from 600°C to 930°C over 3 minutes and holding at the peak temperature for 1 minute, and the completed crowns were allowed to cool to RT.

(6) A layer of approximately 0.5 mm opaque dental porcelain (VITA VMK 68) and then a layer of approximately 1.0 mm dentin porcelain (VITA VMK 95) were PFM fired onto the other three sheet specimens. These three specimens were bench set at RT in each firing cycle. Each specimen with a cross-section of 9 × 5.5 mm^2 was embedded in a resin that was cured from a mixture of 1/3 conducting mounting compound (psi# 212-1; Precision Surfaces International, Houston, TX, USA) and 2/3 epoxy mounting powder (psi# 211-5). The mounted specimens were mechanically polished by sequentially using a series of SiC papers (400—2000 grit), and additionally polished by diamond pastes of 6 μm, 3 μm, and 1 μm, leaving a mirror finish. The surfaces were then carefully wiped with a detergent solution, ultrasonically cleaned in acetone and deionized water, and air dried. Distribution of elements around the interface of ceramic and alloy after two PFM firing cycles was examined using EPMA.

Compressive fracture testing

Compressive fracture tests of ceramometal crowns were performed by using a universal testing machine. A custom-built loading apparatus (Figure S1) was made following the design of Torrado et al.[20] The upper member of the apparatus consisted of a 15-mm-diameter hardened stainless-steel shaft connected to the end of the loading part of a universal testing machine (Model 5582; Instron, Norwood, MA, USA). The opposite end of the shaft was machined to house a 3-mm-diameter loading pin with rounded edges. The pin was secured in place using a lateral setscrew. Only the loading pin contacted the porcelain during testing, and a new pin was used to load each crown. The crown was set on the abutment—analog model mounted on the lower part of the testing machine. An axial load was applied to the inner inclination of buccal and lingual cusps of the occlusal table at the same distance (1.5 mm) from the central groove. Specimens were subjected to a vertical compressive load at a crosshead speed of 0.5 mm/minute until failure to obtain the ultimate fractural strength.

X-ray photoelectron spectroscopy

The outermost part of the oxidized sheet specimens was subjected to XPS analysis using a JAMP-9500F photoelectron

spectrometer (JEOL, Tokyo, Japan), which typically analyzes a depth of 5 nm. An Al Kα X-ray source (1486.6 eV) was obtained using a 10 kV accelerating voltage and a 10 mA filament current. The vacuum level of the analyzing chamber during measurement was of the order of 10^{-10} Torr. The measured binding energies (BEs) were calibrated by referencing the BE of the C 1s line of hydrocarbon contamination (285.0 $\pm$ 0.2 eV).[22] The atomic percentages of Pd, Ag, In, Sn, and Zn on the surface area of the oxidized specimens were calculated according to the relative peak areas, and corrected using Wagner's atomic sensitivity factors.[23]

Scanning electron microscopy/energy dispersive X-ray analysis

The fracture surfaces on both sides of the failed crowns were sputter coated with carbon to produce a thin conductive layer (Cressington 108carbon; Ted Pella Inc., Redding, CA, USA). The oxidized sheet specimens were also coated with carbon after XPS analysis. Morphological features of these specimens were examined using a field emission SEM JSM-6330TF (JEOL) at 10 kV accelerating voltage and 56 μA beam current. An EDX spectrometer (Oxford model 7557; Buck, England) incorporated into the SEM was used to characterize the local elemental composition associated with observed features on the fracture surfaces. EDX spectra were collected from the upper, middle, and lower regions on both sides of the failed crowns, or from different regions of each sheet specimen using an area scan mode. Finally, quantitative EDX area analysis was performed to determine the weight percentage values of Pd, Ag, Zn, Si, Zr, Al, K, and Na, and to calculate the mean values of Pd, Ag, In, Sn, and Zn.

Electron probe microanalysis

A cross-sectioned crown was embedded in resin cured from a mixture of a 1/3 conducting mounting compound (psi# 212-1) and 2/3 epoxy mounting powder (psi# 211-5). The mounted crown was mechanically polished using the same procedures as described for the sheet specimens. These metallographically polished specimens were coated with carbon by sputtering using a carbon coater (Cressington 108carbon). The backscattered electron image (BEI) and secondary electron image were taken over an area of 66 $\times$ 66 μm^2 (1500$\times$) by a JEOL JXA-8900R EPMA at 15 kV and 10^{-8} A. For elemental mapping, the electron beam was scanned over an area of 66 $\times$ 39 μm^2, and simultaneously characteristic X-ray intensities of the corresponding elements were acquired. Elemental concentration profiles in the cross-sectional layer of the ceramic and metal interface were measured using a 1-μm-diameter beam.

Results

Load–displacement plots were acquired during the fracture testing (Figure 2). The maximum load corresponds to the onset of a catastrophic fracture of the crown. Nine load and displacement paired values are listed with plot symbols. The average fractural force was 1425 $\pm$ 392N. A photograph of

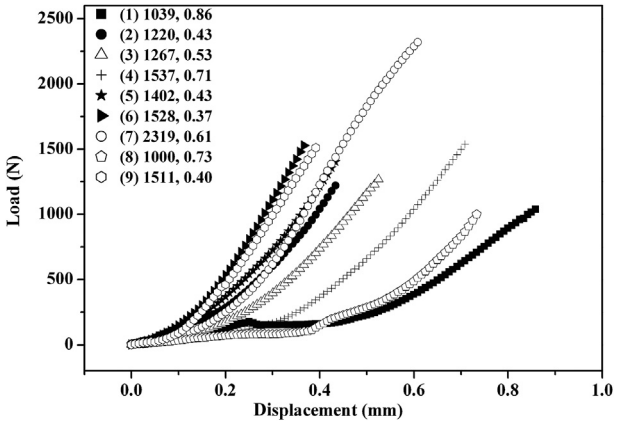

Figure 2 Load against displacement curves from fracture testing.

the fracture surfaces of a representative ceramometal crown is presented in Figure 3). Arrows show the localized areas in filled circles that were analyzed by EDX. The majority of fractures occur in the opaque porcelain layers, with some porcelain remnants being present on the alloy surface.

The three representative BEI micrographs (upper, middle, and lower) and the elemental EDX area scans of the fracture surface on the alloy side show Pd, Ag, Zr, Si, Zn, K, and Al peaks in order of decreasing wt% (Figure S2). For brevity, results on the porcelain side are also not presented here (Figure S3). The elemental composition of the crown's fractural surfaces obtained by EDX analysis is listed in Table 2. Pd, Ag, or Zn was not detected on the porcelain side of the fracture, and no Na was found on the alloy side. The observed composition may not represent a surface phenomenon because the overall depth sampled by EDX is approximately 1 μm. The crown suffered from cohesive failure, with the fracture occurring within the ceramic. The schematic diagram shown in Figure 4 uses solid lines to represent the crack path. The initial crack started at the 3-mm-diameter loading pin/crown interface, propagated

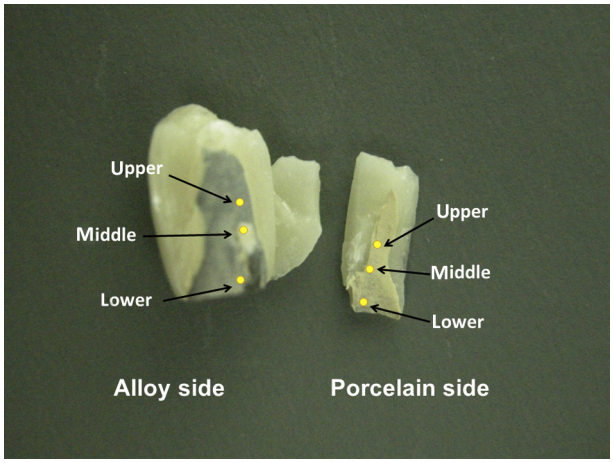

Figure 3 Representative photograph of fractured crown. Arrows show upper, middle, and lower areas for SEM/EDX analysis. EDX Z energy dispersive X-ray spectroscopy; SEM Z scanning electron microscopy.

Table 2 Surface compositions of fractured crown (in wt %).

	Upper area		Middle area		Lower area	
	Alloy side	Porcelain side	Alloy side	Porcelain side	Alloy side	Porcelain side
Pd	32.8	0.0	31.0	0.0	20.4	0.0
Ag	28.5	0.0	30.6	0.0	21.5	0.0
Zn	8.1	0.0	5.8	0.0	9.7	0.0
Si	10.8	32.9	10.8	31.3	15.3	28.0
Zr	12.8	41.0	15.6	40.2	23.5	44.3
Al	3.1	6.8	3.3	7.6	4.3	8.4
K	3.8	12.4	3.0	13.2	5.4	11.7
Na	0.0	6.9	0.0	7.7	0.0	7.6

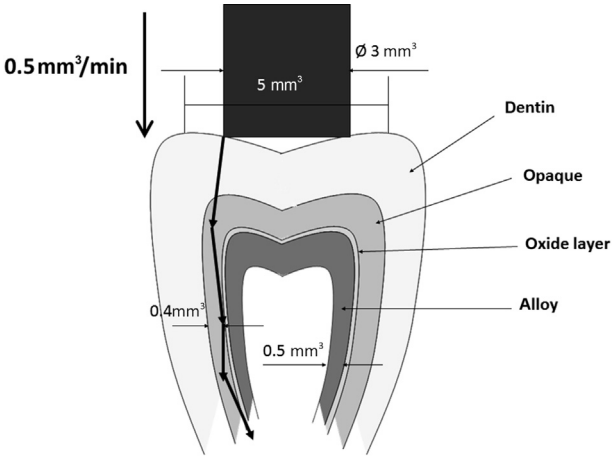

Figure 4 Schematic illustration of the crack path.

through the dentin porcelain layers, spread into the opaque porcelain layers, and then traced a meandering path between the two interfaces (alloy—opaque porcelain and dentin porcelain—opaque porcelain), but remained within the opaque porcelain layer. Finally, the crown fractured as the crack approached the dentin porcelain—opaque porcelain interface.

EPMA was employed to scan the elemental distribution mappings in the metallographically polished specimens after eight PFM firing cycles. A compositional contrast between the alloy and porcelain phases was observed using a backscattering electron detector (Figure S4A). For brevity, Pd and Ag analyses are not presented here, and Sn and In compositions are shown in Figures S4B and S4C, respectively. Sn and In are present only on the alloy side of the specimens, although a more intense In signal is seen along the ceramic—metal boundaries. Zn was located throughout the alloy side and boundary areas, and inside the porcelain (Figure 5). The figure shows a rough surface structure along the boundaries.

A typical survey scan over a BE range of 0—1100 eV for the Pd—Ag alloy sheet after surface oxidation is displayed in Figure 6. This spectrum reveals the presence of Pd, Ag, In, Sn, and Zn. Their atomic concentrations (atom%) based on curve fitting analysis are listed in column 4 of Table 1. For comparison, atom% was converted to wt%, which is listed in column 5 of Table 1. A narrow scan of the Zn 2p line after deconvolution shows two peaks (at 1021.2 eV and 1022.2 eV) originating from the metallic state (Zn^0) and the oxide state (Zn^{2+}), respectively (Figure 7).[22,23] This result indicates the presence of ZnO on the specimen surface. For brevity, the narrow scans of In 3d and Sn 3d are not shown; they reveal the presence of In_2O_3, In, SnO_2, and Sn (Figures S5 and S6).[22—25]

A representative BEI micrograph and its elemental EDX area scan of the oxidized sheet specimen show the Pd, Ag, In, Sn, and Zn peaks (Figures 8 and S7). The results of EDX analysis on the elemental composition of the alloy surfaces are presented in the third column of Table 1. The BEI micrograph and elemental EDX scans for the oxidized alloy indicate that all these elements are evenly distributed over the surface of the specimens (Figure S8). The observed homogeneous distribution is not necessarily a surface phenomenon because the overall depth sampled by EDX is of the order of 1 μm.

The EPMA method was employed to scan the elemental distribution mappings of the metallographically polished sheet specimens after two PFM firing cycles. The compositional contrast between the metal and porcelain phases was observed using backscattered and secondary electron detectors, as presented on the left side of Figure S9. The results of Pd, Ag, and In are illustrated in the middle part, whereas those of Zn and Sn are displayed on the right side. Pd, Ag, In, and Sn elements were distributed only on the metal side of the specimens, and more intense Ag, In, and Sn signals were detected along the metal—porcelain boundaries as compared to Pd. Zn was located on the metal side, and also on the boundary areas and inside the porcelain (Figure 9). The oxidized specimens have a rough surface structure with sharp edges along the boundaries (Figure S9).

Discussion

Owing to the sampling depth of XPS, chemical information is acquired selectively from an ultrathin layer (a few nanometers) on the alloy surface. The problem with SEM/EDX measurements is that the sampled volume is approximately 1 μm in diameter, which prevents extremely thin external oxide layers from being detected. The main advantage of SEM/EDX is that it exhibits favorable spatial resolution. Table 1 shows the mean compositional data based on the EDX and XPS analyses of the Pd/Ag alloy after surface oxidation, as compared with the bulk composition information provided by the manufacturer.

The measured BEs of Pd and Ag (Figure 6) are in good agreement with the reference data of the pure metals[22,23] and remain unchanged after oxidation treatment, as is expected for noble metal alloys. XPS analysis confirmed the presence of the following oxides: In_2O_3, SnO_2, and ZnO. The near-surface accumulation of In_2O_3, SnO_2, and ZnO may be caused by segregation of In, Sn, and Zn from the bulk to the surface of the specimen and subsequent oxidation. This work confirms the research of Brantley et al,[26] who found that alloy surface preparation could have an effect on the surface elements present in the alloy

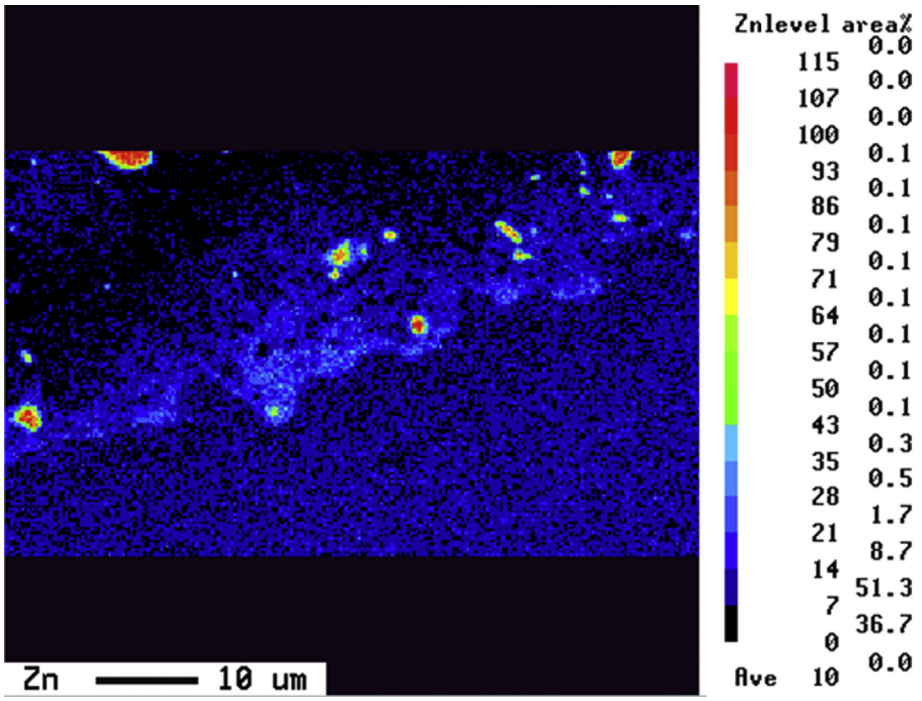

Figure 5 EPMA color photomicrograph showing element distributions of Zn around interface within the crown. EPMA = electron probe microanalysis.

oxide layer, particularly during the oxidation procedure. While firing the ceramic, the alloy was twice heated to 930°C, re-entering a single-phase zone each time. Owing to the high energy at high temperatures, the atoms are enabled to diffuse in the crystal lattice and forced to distribute randomly at the atomic sites (Figure S8). It has been proposed that the mechanism of the resulting enhanced oxide adherence arises from a reduction in the vacancy concentration at the metal–oxide interface.[27] The formation of metal-oxide top layers is essential in bringing elements to the surface that are directly involved in the metal–ceramic bond (In_2O_3, SnO_2, and ZnO). Considering the XPS results, SEM observation, and EPMA analysis, it appears that ZnO was integrated into the ceramic phase as a result of atomic diffusion.

In addition to the chemical bonding between porcelain fused to the alloy interface, micromechanical interlocking was also reported in previous research.[28–31] The advantages of blasting of the alloy surface with Al_2O_3 particles, prior to porcelain application, are increases in surface roughness and surface area. This process has been demonstrated to increase the metal–ceramic adherence.[12,32,33] The micrographs of SEM (Figure S10) and EPMA (Figure S9) provide evidence of mechanical interlocking in this study.

The average and minimum fracture forces (1425 ± 392N and 1000N, respectively) for Pd–Ag ceramometal crowns

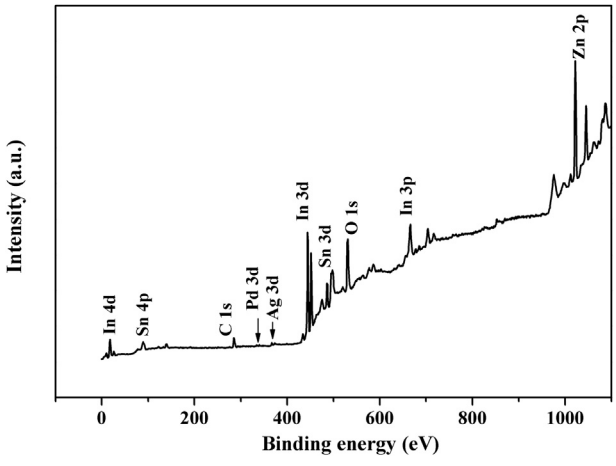

Figure 6 XPS wide scan of alloy after surface oxidation. XPS = X-ray photoelectron spectroscopy.

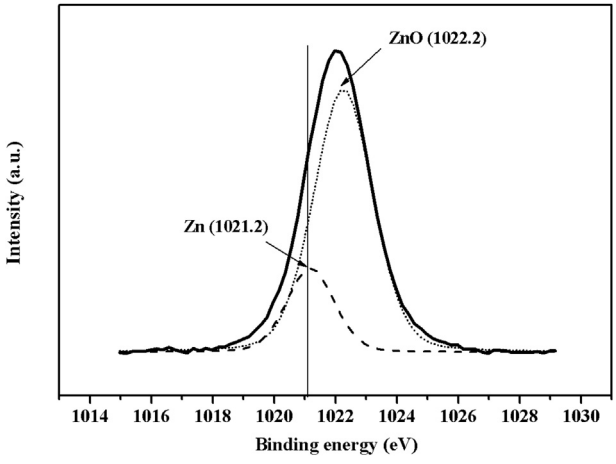

Figure 7 XPS narrow scan of alloy after surface oxidation showing Zn $2p_{3/2}$ peak spread over 1015–1029 eV and covering Zn^0 and ZnO_2. XPS = X-ray photoelectron spectroscopy.

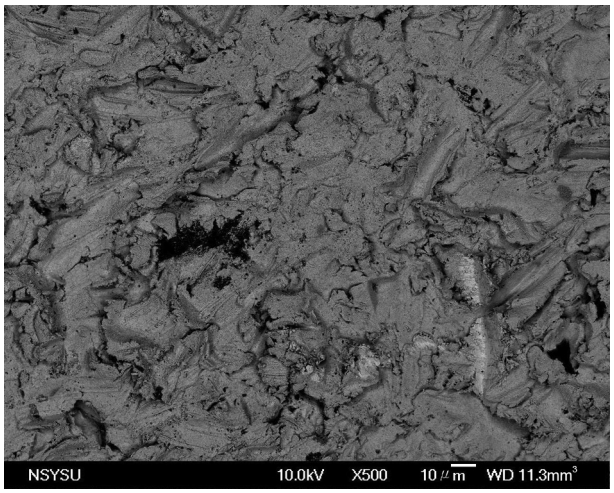

Figure 8 Representative SEM micrograph for oxidized alloy. SEM = scanning electron microscopy.

were substantially greater than the maximal molar region biting force of 847N for men and 597N for women.[9] In the present study, the interface conditions between the crown to abutment and implant analog were assumed to be fully intimate contact for the tested models. However, a completely passive interfacial fit does not usually occur in real clinical situations, and screw designs and rough surfaces of dental implants are dissimilar to each other. These variables for a real dental implant may affect the efficiency of an occlusal load transfer to the surrounding bone, and may cause stress concentration in the occlusal table or at the connection of the abutment and dental implant.[34] Testing casts have their limitations because the biomechanical properties and nonlinear behavior of biological tissues in a real oral cavity cannot be predicted precisely. In the laboratory, the use of a single-cycle load-to-failure and mouth-motion fatigue tests with simplified geometries provide limited data for guiding the development of PFM systems.[10] However, the fracture surface and interface analyses conducted in this study are still vital for successful ceramometal restoration. It is suggested that mechanical interlocking[11–14] contributes to the interface strength based on the rough morphologies seen at the alloy–porcelain boundaries (Figures S4, S9, and S10). Based on the observation that the fractural pathway remained within the opaque porcelain layer and the results from EDX analysis, it is suggested that an adhesive bonding force between the alloy and ceramic is greater than the ceramic cohesive forces. The results from this study are consistent with the findings of other studies.[15,16] Accumulation of easily oxidized elements at ceramic–metal interfaces has been reported in several studies to improve the adherence of porcelain to alloys of noble metals.[17–20,22–24] Such data are generally found to support the chemical bonding mechanisms. In_2O_3 and SnO_2 were found only on the alloy side of the interface, suggesting that they contribute to the interface bond strength. Trace ZnO present at and across the interface is also responsible for improving bonding, and it is suggested that this is a main factor in the observed high fracture resistance of the ceramic–metal interface.

In conclusion, In_2O_3, SnO_2, and ZnO were found along the interface; the presence of these oxides at the boundary promotes ceramic–metal adhesion, and this resulted in cohesive failure of the ceramic layer. ZnO was found to

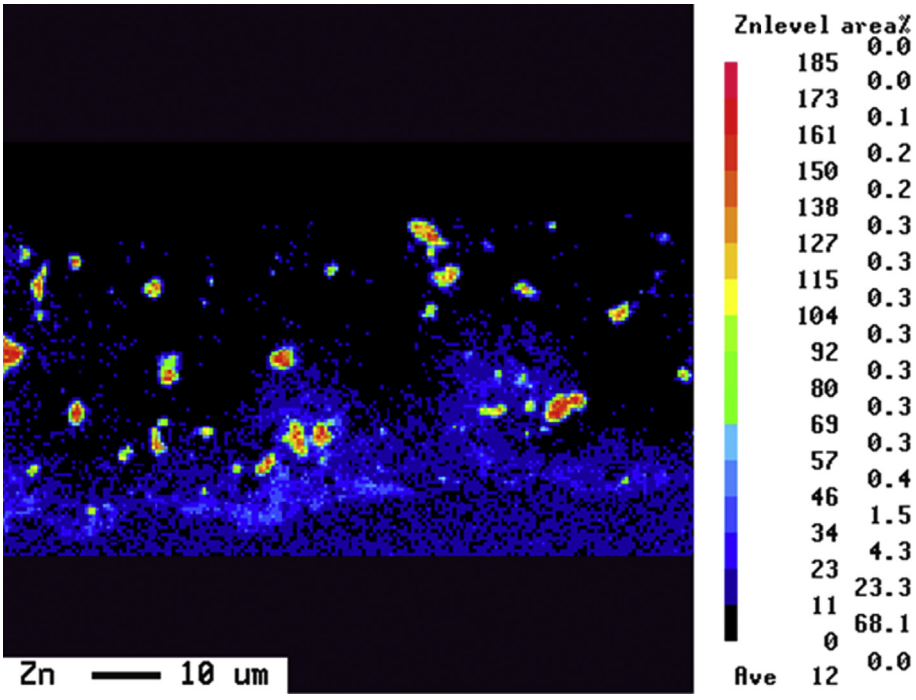

Figure 9 EPMA color photomicrograph showing element distributions of Zn between interface of ceramic and metal after two porcelain-fused-to-metal firing cycles. EPMA = electron probe microanalysis.

diffuse into the ceramic phase, and it is suggested to be beneficial for high fracture resistance in the present study.

Conflicts of interest

The authors have no conflicts of interest relevant to this article.

Acknowledgments

The authors gratefully acknowledge the School of Dentistry, National Yang-Ming University; Department of Materials and Optoelectronic Science, National Sun Yat-sen University; and the Department of Stomatology, Kaohsiung Veterans General Hospital for providing the resources for this study. We would like to thank all the participants of the present study. This study was supported by grants VGHNSU97-005 and VGHNSU98-003 from the Veterans Affairs Commission, Executive Yuan, R.O.C.

Appendix A. Supplementary data

Supplementary data related to this article can be found at http://dx.doi.org/10.1016/j.jds.2015.10.001.

References

1. Huget EF, Civjan S. Status report on palladium—silver-based crown and bridge alloys. *J Am Dent Assoc* 1974;89:383—5.
2. Goodacre CJ. Palladium—silver alloys: a review of the literature. *J Prosthet Dent* 1989;62:34—7.
3. Moffa JP. Alternative dental casting alloys. *Dent Clin North Am* 1983;27:733—46.
4. Nally JN, Monnier D, Meyer JM. Topographic distribution of certain elements of alloy and porcelain at the level of the ceramic and metallic bond. *SSO Schweiz Monatsschr Zahnheilkd* 1968;78:868—78.
5. Ohno H, Ichikawa T, Shiokawa N, Ino S, Iwasaki H. ESCA study on the mechanism of adherence of metal to silica glass. *J Mater Sci* 1981;16:1381—90.
6. Hautaniemi JA. The effect of indium on porcelain bonding between porcelain and Au—Pd—In alloy. *J Mater Sci Mater Med* 1995;6:46—50.
7. Bagby M, Marshall SJ, Marshall Jr GW. Effects of porcelain application procedures on two noble alloys. *J Appl Biomater* 1990;1:31—7.
8. Papazoglou E, Brantley WA, Mitchell JC, Cai Z, Carr AB. New high-palladium casting alloys: studies of the interface with porcelain. *Int J Prosthodont* 1996;9:315—22.
9. Vrijhoef MMA, Van Der Zel JM. Oxidation of a gold—palladium PFM alloy. *J Oral Rehabil* 1988;15:307—12.
10. Hautaniemi JA, Heinonen M, Juhanoja J. Characterization of a surface-treated Au—Ag—Cu-based dental metal—ceramic alloy. *Surf Interface Anal* 1995;23:833—43.
11. Shell JS, Nielsen JP. Study of the bond between gold alloys and porcelain. *J Dent Res* 1962;41:1424—37.
12. Carter JM, Al-Mudafar J, Sorensen SE. Adherence of a nickel—chromium alloy and porcelain. *J Prosthet Dent* 1979;41:167—72.
13. Mackert JR, Ringle RD, Parry EE, Evans AL, Fairhurst CW. The relationship between oxide adherence and porcelain—metal bonding. *J Dent Res* 1988;67:474—8.
14. Anusavice KJ. *Phillips' Science of Dental Materials*, 12th ed. St Louis: Saunders, 2012:377—82.
15. Kinsel RP, Lin D. Retrospective analysis of porcelain failures of metal ceramic crowns and fixed partial dentures supported by 729 implants in 152 patients: patient-specific and implant-specific predictors of ceramic failure. *J Prosthet Dent* 2009;101:388—94.
16. Strub JR, Stiffler S, Schärer P. Cause of failure following oral rehabilitation: biological versus technical factors. *Quintessence Int* 1988;19:215—22.
17. Galindo DF, Ercoli C, Graser GN, Tallents RH, Moss ME. Effect of soldering on metal—porcelain bond strength in repaired porcelain-fused-to-metal casting. *J Prosthet Dent* 2001;85:88—94.
18. Park JS, Kim HS, Kim HSL, Son MK, Choe HC. Interfacial bonding and fracture phenomena between porcelain and metal coping. *Procedia Eng* 2011;10:1567—72.
19. Kang MS, Ercoli C, Galindo DF, Graser GN, Moss ME, Tallents RH. Comparison of the load at failure of soldered and nonsoldered porcelain-fused-to-metal crown. *J Prosthet Dent* 2003;90:235—40.
20. Torrado E, Ercoli C, Al Mardini M, Graser GN, Tallents RH, Cordaro L. A comparison of the porcelain fracture resistance of screw-retained and cement-retained implant-supported metal-ceramic crowns. *J Prosthet Dent* 2004;91:532—7.
21. Chang HS, Chen M, Hsieh YD, Wu HJ. Fractural strength of porcelain fused to metal systems. *J Acad Oper Dent* 2011;2:11—22 [In Chinese, English abstract].
22. Briggs D, Seah MP, eds. *Practical Surface Analysis by Auger and X-Ray Photoelectron Spectroscopy*, 2nd ed. New York: Wiley, 1990.
23. Wagner CD. *Handbook of X-Ray Photoelectron Spectroscopy: A Reference Book of Standard Data for Use in X-ray Photoelectron Spectroscopy*. Minnesota: Perkin-Elmer Corp, 1979.
24. Lin AWC, Armstrong NR, Kuwana T. X-ray photoelectron/Auger electron spectroscopic studies of tin and indium metal foils and oxides. *Anal Chem* 1977;49:1228—35.
25. Cox PA, Egdell RG, Harding C, Patterson WR, Tavener PJ. Surface properties of antimony-doped tin(IV) oxide: a study by electron-spectroscopy. *Surf Sci* 1982;123:179—203.
26. Brantley WA, Cai Z, Papazoglou E, et al. X-ray diffraction studies of oxidized high-palladium alloys. *Dent Mater* 1996;12:333—41.
27. Wu Y, Moser JB, Jameson LM, Malone WFP. The effect of oxidation heat treatment of porcelain bond strength in selected base metal alloys. *J Prosthet Dent* 1991;66:439—44.
28. Carpenter MA, Goodkind RJ. Effect of varying surface texture on bond strength of one semiprecious and one nonprecious ceramo-alloy. *J Prosthet Dent* 1979;42:86—95.
29. Wagner WC, Asgar K, Bigelow W, Flinn RA. Effect of interfacial variables on metal—porcelain bonding. *J Biomed Mater Res* 1993;27:531—7.
30. Okazaki M, Wang X, Toguchi MS, et al. Improvement of bond strength in metal-ceramic systems using a gold intermediate layer. *Dent Mater J* 1998;17:163—73.
31. Vasani R, Kawashima I, Ziebert GJ, Berzins DW. Metal—ceramic interface evaluation of a gold-infiltrated alloy. *J Prosthodont* 2009;18:560—5.
32. Papadopoulos T, Tsetsekou A, Eliades G. Effect of aluminium oxide sandblasting on cast commercially pure titanium surfaces. *Eur J Prosthodont Restor Dent* 1999;7:15—21.
33. Papadopoulos T, Tsetsekou A, Eliades G. Effect of Al_2O_3 sandblasting on casted cpTi surfaces. *J Dent Res* 1998;77:1245.
34. Chang HS, Chen YS, Hsieh YD, Hsu ML. Stress distribution of two commercial dental implant systems: a three-dimensional finite element analysis. *J Dent Sci* 2013;8:261—71.